Restoring the valence-shell stabilization in ^{140}Nd

R. Kern[1], R. Zidarova[1,2], N. Pietralla[1], G. Rainovski[2], R. Stegmann[1], A. Blazhev[3], A. Boukhari[4], J. Cederkäll[4,5],
J. G. Cubiss[6], M. Djongolov[2], C. Fransen[3], L. P. Gaffney[4,7], K. Gladnishki[2], E. Giannopoulos[4,8,9], H. Hess[3],
J. Jolie[3], V. Karayonchev[3], L. Kaya[3], J. M. Keatings[10,11], D. Kocheva[2], Th. Kröll[1], O. Möller[1], G. G. O'Neill[12,13],
J. Pakarinen[8,9], P. Reiter[3], D. Rosiak[3], M. Scheck[10,11], J. Snall[5], P.-A. Söderström[1,14], P. Spagnoletti[10,11],
M. Stoyanova[2], S. Thiel[3], A. Vogt[3], N. Warr[3], A. Welker[4], V. Werner[1], J. Wiederhold[1], and H. De Witte[15]

[1] *Technische Universität Darmstadt, Department of Physics,*
Institut für Kernphysik, 64289 Darmstadt, Germany
[2] *Faculty of Physics, St. Kliment Ohridski University of Sofia, 1164 Sofia, Bulgaria*
[3] *Institut für Kernphysik, Universität zu Köln, 50937 Cologne, Germany*
[4] *ISOLDE, CERN, 1211 Geneva 23, Switzerland*
[5] *Department of Nuclear Physics, University of Lund, 221 00 Lund, Sweden*
[6] *Department of Physics, University of York, York YO10 5DD, United Kingdom*
[7] *Oliver Lodge Laboratory, University of Liverpool, L69 7ZE Liverpool, United Kingdom*
[8] *Helsinki Institute of Physics, University of Helsinki, P.O. Box 64, FIN-00014 Helsinki, Finland*
[9] *Department of Physics, University of Jyvaskyla, P.O. Box 35, 40014 Jyvaskyla, Finland*
[10] *CEPS, University of the West of Scotland, Paisley PA1 2BE, United Kingdom*
[11] *SUPA, Scottish Universities Physics Alliance, United Kingdom*
[12] *Department of Physics, University of Western Cape, Bellville 7535, South Africa*
[13] *iThemba LABS, National Research Foundation, Somerset West 7129, South Africa*
[14] *Extreme Light Infrastructure-Nuclear Physics (ELI-NP)/Horia Hulubei*
National Institute for R&D in Physics and Nuclear Engineering,
Str. Reactorului 30, 077125 Bucharest-Măgurele, Romania and
[15] *Instituut voor Kern- en Stralingsfysica, K.U. Leuven, 3001 Leuven, Belgium*
(Dated: October 19, 2020)

A projectile Coulomb-excitation experiment was performed at the radioactive-ion beam facility HIE-ISOLDE at CERN to obtain $E2$ and $M1$ transition matrix elements of ^{140}Nd using the multi-step Coulomb-excitation code GOSIA. The absolute $M1$ strengths, B$(M1; 2_2^+ \rightarrow 2_1^+) = 0.033(8)\,\mu_N^2$, B$(M1; 2_3^+ \rightarrow 2_1^+) = 0.26^{+0.11}_{-0.10}\,\mu_N^2$, and B$(M1; 2_4^+ \rightarrow 2_1^+) < 0.04\,\mu_N^2$, identify the 2_3^+ state as the main fragment of the one-quadrupole-phonon proton-neutron mixed-symmetry state of ^{140}Nd. The degree of F-spin mixing in ^{140}Nd was quantified with the determination of the mixing matrix element $V_{\mathrm{F-mix}} < 7^{+13}_{-7}\,$keV.

The present day understanding of the structure of excited nuclear states is shaped by two extreme concepts, namely those of single-particle and collective motions. The single-particle motion reflects the quantum nature of atomic nuclei. The basic framework for understanding the single-particle motion is provided by the nuclear shell model with the spin-orbital interaction [1], which leads to the existence of discrete quantum states characterized by their total (j) and orbital (l) angular momenta. The states are grouped in shells leading to the existence of magic numbers. The collective motion is a coherent movement of groups of few or many nucleons caused by the residual interaction, dominated by the proton-neutron interaction [2]. It reflects the many-body character of atomic nuclei [3] and can geometrically be described by considering the nucleus as a homogeneous system, which vibrates or rotates [4].

In general, large-scale shell-model calculations with realistic interactions could provide a description of the collective excitations in the fundamental framework of the nuclear shell model. However, for heavy open-shell nuclei this approach runs into computational problems due to the fact that it requires enormously large configuration spaces. The Interacting Boson Model (IBM) was introduced by F. Iachello and A. Arima [5] as an effective approximation used to avoid this problem. It repre-

sents a severe truncation of the shell model. Its original (sd-IBM-1) version is designed to describe quadrupole-collective excitations of even-even nuclei. The basic principle of the IBM-1 is, that the nucleons are separated in an inert core and valence nucleons. The inert core is taken to be the closest doubly-magic nucleus. The valence nucleons couple pairwise to bosons and are solely responsible for the excitations of the nucleus. In the IBM-1, no distinction between valence-proton and valence-neutron bosons is made and as a result they are interchangeable.

Besides the quantum nature and the many-body aspect, the uniqueness of the atomic nucleus as a dynamical system is also determined by its two-fluid character. This feature is taken into account in the IBM-2 [6], where separated proton and neutron bosons are introduced. The types of bosons are not always interchangeable. As a result, two distinctive classes of excitations appear. The states of the first one, where proton and neutron bosons are coupled symmetrically, are called full-symmetry states (FSSs) and, in fact, they are states which appear in the framework of IBM-1. The second class of states has wave functions in which at least one pair of proton and neutron bosons are coupled anti-symmetrically. These states are called mixed-symmetry states (MSSs). The discovery of the so-called scissors

mode ($J^\pi = 1^+$) of the axially deformed nucleus ^{156}Gd by Bohle *et al.* [7] was the first experimental evidence of MSSs.

In the framework of the IBM-2 the F spin is introduced to quantify the degree of coherence of the proton-boson and neutron-boson contribution of the state's wave function. F spin for bosons is analogous to isospin for nucleons. The maximum F spin of a state is $F_{\max} = (N_\pi + N_\nu)/2$, where N_π and N_ν are the number of valence-proton and valence-neutron bosons, respectively. The F spin of FSSs is $F = F_{\max}$, whereas the F spin of all observed MSSs is $F = F_{\max} - 1$. According to the IBM-2, the mixed-symmetry one-quadrupole-phonon state ($2^+_{1,\mathrm{ms}}$) is the lowest-lying MSS of heavy vibrational nuclei [8]. The isovector ($\Delta F = 1$) nature of the transition between the $2^+_{1,\mathrm{ms}}$ state and the fully-symmetric 2^+_1 state leads to the distinctive strong $M1$ connection – i.e., an absolute transition strength of B($M1; 2^+_{1,\mathrm{ms}} \to 2^+_1$) $\approx 0.2\,\mu_N^2$ is expected [8]. In contrast, the $M1$ strength of an isoscalar transition between FSSs ($\Delta F = 0$) is highly suppressed and the corresponding $M1$ transition strength is an order of magnitude lower. In addition, the one-quadrupole-phonon structure of the $2^+_{1,\mathrm{ms}}$ state leads to a weakly collective $E2$ transition (≈ 1 W.u.) to the ground state [8].

The gradual evolution of nuclear properties as a function of the nucleon number within major shells and sudden changes, which appear at magic numbers, can well be understood in the frameworks of both collective and microscopic single-particle models. One could expect that these general trends in the collective properties within the major shells are modulated by the sub-shell structure. However, it is usually thought that the pairing correlations smear out and dissolve the effects from the sub-shell structure making them difficult to detect, especially in the case of FSSs. It has been suggested, however, that the properties of MSSs are more sensitive to the underlying sub-shell structure through a mechanism dubbed "*valence-shell stabilization* of nuclear isovector excitations" [9].

The observation of isolated $2^+_{1,\mathrm{ms}}$ states for the $N = 80$ isotones $^{132}_{52}$Te, $^{134}_{54}$Xe and $^{136}_{56}$Ba [10–12], was explained by the partly filled $\pi g_{7/2}$ orbital. This results in a *valence-shell stabilization* of one-quadrupole-phonon isovector excitations, but this effect disappears once the $\pi g_{7/2}$ orbital is fully occupied. The lack of *valence-shell stabilization* is manifested by a fragmentation of the one-quadrupole-phonon MSS. Indeed, a fragmented $2^+_{1,\mathrm{ms}}$ state is observed in ^{138}Ce ($Z = 58$) [9]. The fragmentation implies the breaking of the F-spin symmetry and consequently a significant mixing of MSSs with FSSs. The process can be quantified by the magnitude of the mixing matrix element ($V_{\mathrm{F-mix}}$), which can be derived from the experimental data on the absolute $M1$ and $E2$ transition strengths of the decays of the involved states [9]. While small matrix elements $V_{\mathrm{F-mix}}$ are derived in the cases of single isolated $2^+_{1,\mathrm{ms}}$ states, a large one is extracted in the case of ^{138}Ce [9].

Providing that the mechanism of *valence-shell stabi-lization* is qualitatively correct, one can expect that it will be restored for the $N = 80$ isotones once the quadrupole excitations begin to develop predominantly in the $\pi d_{5/2}$ orbital. As a consequence of this, a single isolated one-quadrupole-phonon MSS can be expected in ^{140}Nd. However, it has to be noted that an unambiguous identification of MSSs in unstable nuclei can at present, solely be achieved in Coulomb excitation (CE) experiments of post-accelerated radioactive-ion beams (RIB) [11, 13, 14]. Therefore, in order to investigate this prediction of the *valence-shell stabilization* mechanism a projectile CE experiment was performed with the RIB of ^{140}Nd at HIE-ISOLDE at CERN [15, 16].

In the reported CE experiment at HIE-ISOLDE at CERN, radioactive atoms were produced by bombarding a thick tantalum target with high-energy protons (1.4 GeV) from the PS-Booster. A wide variety of isotopes was produced by the occurring fission, spallation, and fusion reactions, which were subsequently ionized by a hot surface ion source. In addition, the selective laser ionization system, RILIS [18], was applied to increase the ionization rate of neodymium atoms. The first ionization process was followed by the mass selection in the General Purpose Separator (GPS) and charge breeding in an electron-beam ion source, REXEBIS [17]. The efficiency of the delivery of ^{140}Nd ions from the ion source to the post-acceleration section was 8%. The radioactive ions were post-accelerated up to 4.62 MeV/A through the REX and HIE cavities [15, 16] and were delivered to the Miniball [19] experimental station with a transmission of about 79%. Finally, approximately 1.3×10^6 ^{140}Nd ions per seconds impinged on a 1.5 mg·cm^{-2}-thick ^{208}Pb target. The beam energy was chosen to be sufficiently low to consider the reaction of ^{140}Nd and ^{208}Pb as "safe" CE – i.e., the distance between the surfaces of both reaction partners was greater than 5 fm [21]. The scattered charged particles were detected by a double-sided silicon strip detector (DSSD) [19, 20], which was mounted in
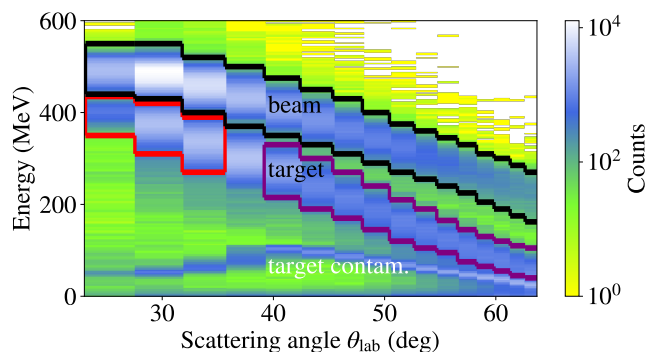

FIG. 1. The spectrum of the double-sided silicon strip detector shows the energy of the scattered heavy particles as a function of the scattering angle with respect to the beam axis (laboratory frame). Three different types of particles, heavy target, light target (contamination), and beam particles, are clearly separated. The gate for target-like particles is divided in single-hit (red) and double-hit (purple) events.
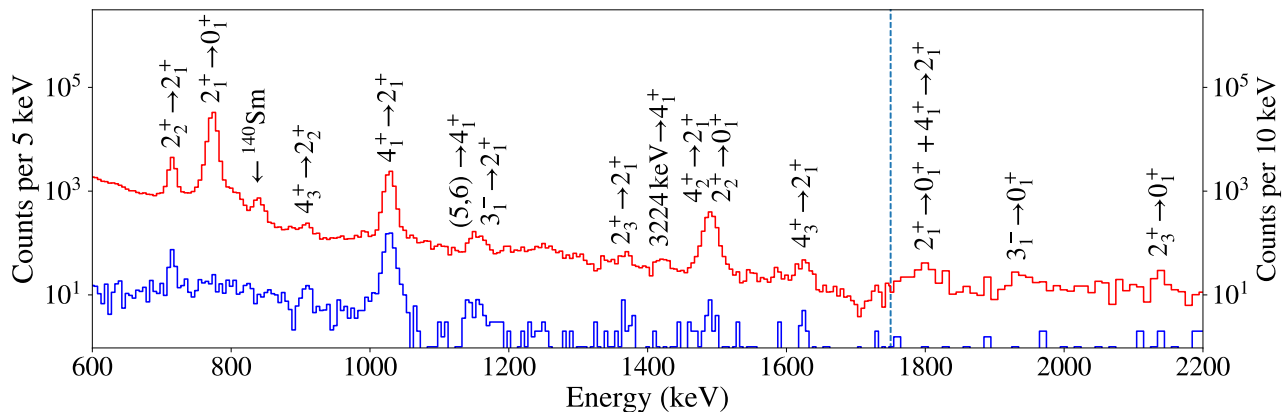
FIG. 2. The time-random background subtracted, Doppler-corrected, beam-particles gated γ-ray singles spectrum (red) and the γ-ray coincidence spectrum (blue) with an additional gate on the $2_1^+ \rightarrow 0_1^+$ transition of ^{140}Nd. Peaks are marked with the identified transition emitted following the CE of ^{140}Nd. Additionally, a peak at 840 keV was identified as a transition of the beam contaminant ^{140}Sm, which vanishs in the γ-ray coincidence spectrum. The binning changes after the dashed line for visibility.

forward direction covering the angles between 24.0 ° and 63.7 ° with respect to the beam axis.

The Miniball-DSSD events were built by using the sorting code from Ref. [22]. In total, 1.2×10^6 single-hit and 7.8×10^5 double-hit events were recorded on the DSSD. The 2D histogram of the particle energy in dependence of the scattering angle (cf. FIG. 1) is used for the differentiation of beam- or target-like particles hitting the DSSD. The two-particle events, which involve a beam particle as well as the corresponding reaction partner (target-like particle), are solely assigned to beam-like particle events to avoid double counting. However, single-hit target-like events are also detected in the range where two-particle events are expected. These cases happen, if the beam-like reaction partner is lost to the inter-strip boundaries of the detector, subject to pile-up or otherwise not detected. Therefore, the acceptance of the single-hit target gate was limited to the three inner rings of the DSSD. Here, the beam-like reaction partner was scattered outside the angles of the DSSD. Hence, the potential corruption of the cross sections of target-gated spectra is prevented. Thus, this limitation enabled us to measure the unpeturbed CE cross sections of the target-gated and beam-gated events.

The depopulating γ rays of the Coulomb-excited states were recorded by Miniball, in total 1.1×10^5 events with the condition for a detection of a target-like and 8.4×10^5 events for a beam-like recoil. Miniball consisted during the experiment of 24 six-fold segmented high-purity Germanium detectors. The most prominent contamination in the γ-ray singles spectrum originated from the CE of ^{140}Sm. The ratio of ^{140}Sm in the beam could be successfully suppressed by using RILIS to approximately 50 % relative to the number of ^{140}Nd ions. The γ-ray singles spectrum is dominated by the $2_1^+ \rightarrow 0_1^+$ transition at 774 keV with an energy resolution of 1.4 % (FWHM = 11 keV) after an event-by-event Doppler-shift correction, cf. FIG. 2. In total, depopulating γ rays of three ex-
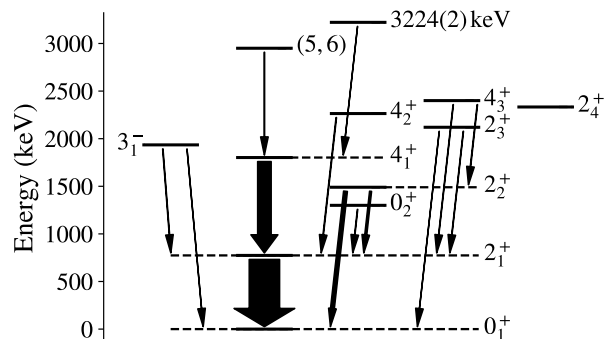

FIG. 3. The partial level scheme of ^{140}Nd. The widths of the transitions correspond to the observed intensities. The $2_1^+ \rightarrow 0_1^+$ transition width is scaled down by a factor of 5 for visibility.

cited 2^+, a 3^-, three 4^+ and two higher-lying states with unknown spin assignment were observed, cf. FIG. 3.

The CE analysis has been performed with the multi-step CE code GOSIA [23]. GOSIA reproduces the observed population yields of excited states with a given set of transition matrix elements, that are responsible for the CE, in this case mostly $E2$ and $E3$ transitions. The electron conversion [24], the energy loss of the charged particles in the target [25], and the detector geometries are taken into account. The measured experimental yields are normalized to the CE cross section of the 2_1^+ state, which is determined by the known absolute $E2$ transition strength B($E2; 2_1^+ \rightarrow 0_1^+$) = 33.6(27) W.u. and the diagonal matrix element $\langle 2_1^+ || E2 || 2_1^+ \rangle = -0.64\,(48)$ eb of ^{140}Nd [26]. Knowledge about the multipole-mixing ratios of the $2_i^+ \rightarrow 2_1^+$ transitions, $\delta(2_{2,3,4}^+ \rightarrow 2_1^+) = -1.22(14), -0.08(8),$ and $-0.19(9)$ [27], is indispensable for the determination of the sought-for absolute $M1$ transition strengths. The observed level scheme (cf. FIG 3) and additional so-called buffer states, above the levels of

interest, are included in the GOSIA input. The transition matrix elements are determined by a fit to the yields of both, beam-gated and target-gated events, simultaneously. Both sets of experimental yields are reproduced inside their one-sigma uncertainties. These experimental data are not sensitive to the signs of the transition matrix elements except for three matrix elements involved in the excitation of the 4_3^+ state at 2400 keV, $\langle 2_1^+||E2||2_2^+\rangle$, $\langle 2_1^+||E2||4_3^+\rangle$, and $\langle 2_2^+||E2||4_3^+\rangle$, and the ground state matrix element of the 3_1^- state, $\langle 0_1^+||E3||3_1^-\rangle$. This leads to several reasonable solutions, which results in additional systematical uncertainties of all matrix elements. These are included in the total uncertainties together with the statistical uncertainties. The resulting $M1$, $E2$ and $E3$ transition strengths are shown in TABLE I.

The most promising candidate for the main fragment of the $2_{1,ms}^+$ state is the 2_3^+ state. 113 and 12 γ-ray events of its predominant decay to the 2_1^+ state at 1366 keV are observed in the beam-particle-gated γ-singles and coincidence spectrum, respectively. Furthermore, 33 γ-ray events of the ground state transition at 2140 keV, which was unobserved before, were counted (cf. FIG. 2). A χ^2-surface analysis has been performed to obtain the correlation of the two $E2$ transition matrix elements, which are primarily responsible for the CE of the 2_3^+ state, $\langle 0_1^+||E2||2_3^+\rangle$ and its diagonal matrix element $\langle 2_3^+||E2||2_3^+\rangle$, cf. FIG. 4. The same diagonal $E2$ matrix element of the 2_3^+ state, as it is known for the 2_1^+ state, is applied as an additional data point to the analysis. The χ^2-surface distribution in FIG. 4 shows the strong correlation of these two matrix elements and it is used to determine the uncertainty of $\langle 0_1^+||E2||2_3^+\rangle$.

The resulting matrix element $\langle 0_1^+||E2||2_3^+\rangle$ = 0.204 (34) eb, the branching ratio of the depopulating γ-ray transitions of the 2_3^+ state, $I_{2_3^+\to 0_1^+}/I_{2_3^+\to 2_1^+}$ = 0.38 (11), and the multipole-mixing ratio [27] lead to the absolute $M1$ transition strength of B($M1; 2_3^+ \to 2_1^+$) = 0.26 (11) μ_N^2. The lower uncertainty is reduced by the known upper limit $I_{2_3^+\to 0_1^+}/I_{2_3^+\to 2_1^+}$ < 0.42 [27]. The analogous procedure has been conducted for the 2_4^+ state. Decays of the 2_4^+ state are unobserved in this experiment, hence, an upper limit of B($M1; 2_4^+ \to 2_1^+$) < 0.04 μ_N^2 is deducted by assuming an intensity of the $2_4^+ \to 2_1^+$ and $2_4^+ \to 0_1^+$ transitions at the edge of the detection limit. The known branching ratio $I_{2_4^+\to 0_1^+}/I_{2_4^+\to 2_1^+}$ = 1.9 (6) [31] is applied to the calculation. The resulting $M1$- and $E2$-strength distributions are displayed in FIG. 5.

Various IBM-2, large-scale shell model (LSSM), and quasi-particle phonon model (QPM) calculations were carried out to reproduce and predict the $M1$-strength evolution of the $N = 80$ isotones [32–34]. Using a modified pairing strength, Sieja *et al.* [33] succeeded in accurately describing the $M1$ strengths of the MSSs of $N = 80$ isotones from ^{132}Te to ^{138}Ce, while predicting an increase of the $M1$ strength from ^{138}Ce to ^{140}Nd. The model predicted a B($M1; 2_{MSS}^+ \to 2_1^+$) $\approx$ 0.2 μ_N^2 at around 2.3 MeV (cf. FIG. 6) for ^{140}Nd.

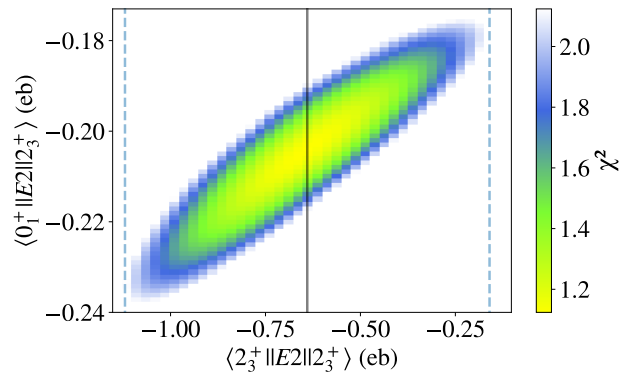The $2_{3,4}^+$ states of ^{140}Nd at 2.140 and 2.332 MeV,

FIG. 4. χ^2-surface distribution with respect to the diagonal and transitional matrix elements of the 2_3^+ state. The dashed gray lines indicate the limits of the diagonal matrix element of the 2_1^+ state, which is applied to the 2_3^+ state.

respectively, were experimentally identified as the two fragments of the $2_{1,ms}^+$ state due to their predominant $M1$ transitions to the 2_1^+ state [27]. The result of B($M1; 2_3^+ \to 2_1^+$) = $0.26^{+0.11}_{-0.10}\,\mu_N^2$ indicates that the 2_3^+ state is the main fragment of the MSS. This is also in good agreement with the theoretical predictions from Ref. [33] (LSSM) and from Ref. [30] (QPM). Hence, the 2_4^+ state can be adopted, at most, as the minor fragment of the $2_{1,ms}^+$ state.

The F-spin mixing matrix element is determined to quantify the degree of mixing of the F spin in ^{140}Nd. The simplest scenario is a two-state mixing, where the $M1$ strength between two FSSs is zero, according to the IBM-2. However, the concept of idealized FSSs is an approximation and does not reflect reality. Therefore the $M1$ connection between nuclear states, which are labeled as FSSs, is not strictly forbidden, though it is highly suppressed. This general non-zero $M1$ strength between FSSs is determined by the B($M1; 2_2^+ \to 2_1^+$) = 0.033(8) μ_N^2 assuming the 2_2^+ state as a pure FSS. Thus, a more realistic mixing scenario is applied, where the $M1$ strength between FSSs interferes constructively with the $M1$ strength between a MSS and a FSS. This results in a F-spin mixing matrix element of V_{F-mix} < 7^{+13}_{-7} keV. This clearly indicates a decrease of the strength of the F-spin mixing from ^{138}Ce to ^{140}Nd, in contrast to the calculations (V_{F-mix} = 92 (14) keV) from Ref. [27], which were solely based on multipole-mixing ratios. This decrease displays the observed evolution of these isotones' B($M1; 2_i^+ \to 2_1^+$) distributions, cf. FIG. 6: the ratio of the $M1$ strengths of the small fragment and the main fragment in ^{138}Ce is approximately 1/2, whereas it is less than 1/8 in 140Nd. So the F-spin mixing is obviously reduced again when passing the $Z = 58$ sub-shell closure.

Looking at the evolution of V_{F-mix} for the $N = 80$ isotones (cf. FIG. 6), the strong mixing of ^{138}Ce V_{F-mix} = $44(3)^{+4}_{-11}$ keV [9] clearly stands out. The V_{F-mix} of ^{134}Xe is calculated under the same assumptions as in ^{140}Nd, namely a $M1$ strength between FSSs of B($M1; 2_2^+ \to$

TABLE I. Measured properties of the levels and γ-ray transitions of ^{140}Nd. Level energies and spin assignments are adopted from Ref. [28] unless otherwise noted. The relative γ-ray intensities determined from the beam-gated (exp. 1) and the target-gated (exp. 2) γ-ray spectra are corrected for efficiency.

E_{level} (keV)	J^π	E_γ (keV)	J_f^π	I_γ exp. 1	I_γ exp. 2	δ from [27]	$\pi\lambda$	$B(\pi\lambda)\downarrow$ [a]
774	2_1^+	774	0_1^+	100(1)	100(1)		E2	33.6(27)[b]
1413	0_2^+	639	2_1^+	0.3(1)	1.4(4)		E2	7.5(16)[c]
1490	2_2^+	1490	0_1^+	2.1(1)	5.5(6)		E2	1.76(13)
		716[d]	2_1^+	1.6(2)	2.7(8)	-1.22(14)	E2	33(3)
							M1	0.033(8)
1802	4_1^+	1028[d]	2_1^+	9.6(1)	21.4(6)		E2	40(1)
1936	3_1^-	1936	0_1^+	0.08(2)			E3	6(2)
		1162[d]	2_1^+	0.25(4)	0.9(4)			
2140	2_3^+	2140	0_1^+	0.07(2)			E2	1.9(6)
		1366[d]	2_1^+	0.19(3)		-0.08(8)	E2	$0.3^{+0.6}_{-0.3}$
							M1	$0.26^{+0.11}_{-0.10}$
2264	$4_2^{+\,\text{e}}$	1491[d]	2_1^+	0.4(1)	1.2(5)		E2	2.3(8)
2333	2_4^+	2333	0_1^+	< 0.03			E2	<0.8
		1560	2_1^+	< 0.03		-0.19(9)	E2	<0.4
							M1	<0.04
2400	4_3^+	1626[d]	2_1^+	0.21(4)			E2	1.6(3)
		910[d]	2_2^+	0.31(5)			E2	41(7)
2950[f]	$(5,6)^{\text{e}}$	1148[gh]	4_1^+	0.40(6)	1.6(5)		E2	30(3)
3224[f]		1422[gh]	4_1^+	0.17(3)	1.0(2)		E2	22(4)

[a] $B(M1)$ values are given in μ_N^2, $B(E2)$ and $B(E3)$ values are given in W.u. ($E2$: 1 W.u. $= 4.32 \times 10^{-3}$ e^{2}b^2; $E3$: 1 W.u. $= 1.16 \times 10^3$ e^{2}b^3)

[b] Transition strength adopted from Ref. [26]

[c] This value is extracted without considering $E0$ excitation. It has to be considered as an estimate only

[d] Observed in coincidence spectrum of the $2_1^+ \to 0_1^+$ transition

[e] Spin adopted from Ref. [29]

[f] Assumed as a 6^+ state in the GOSIA analysis

[g] Observed in coincidence spectra of the $4_1^+ \to 2_1^+$ and $2_1^+ \to 0_1^+$ transitions

[h] Transition energy adopted from Ref. [30]

FIG. 5. The values for B($M1; 2_i^+ \to 2_1^+$), B($E2; 2_i^+ \to 2_1^+$) and B($E2; 2_i^+ \to 0_1^+$) strengths of ^{140}Nd are displayed in a), b) and c), respectively.

FIG. 6. The $M1$ transition strengths B($M1; 2_1^+ \to 2_1^+$) of the main and the small fragment of the $2_{1,\text{ms}}^+$ state of the $N = 80$ isotones are compared to a theoretical B($M1; 2_{1,\text{ms}}^+ \to 2_1^+$) systematic (Sieja $et\ al.$, 2009: Ref. [33]) in a). The resulting F-spin mixing matrix elements ($\circ$) and upper limits ($\triangledown$) are shown in b). $V_{\text{F}-\text{mix}}$ of ^{136}Ba and ^{138}Ce are taken from Ref. [9].

2_1^+) $= 0.033\,(8)\,\mu_N^2$, and with spectroscopic information taken from [10]. This results in $V_{\text{F}-\text{mix}} = 12^{+18}_{-12}$ keV for ^{134}Xe. The evolution of the fragmentation of the MSSs from ^{134}Xe to ^{140}Nd shows a restauration of the $valence$-$shell\ stabilization$ for the even-even $N = 80$ isotones at ^{140}Nd and indicates the F spin as a well conserved quantum number for the $N = 80$ isotones apart from the sub-shell closure at $Z = 58$.

In summary, a projectile CE experiment was performed at HIE-ISOLDE at CERN to determine absolute $M1$ transition strengths B($M1; 2_i^+ \to 2_1^+$) of ^{140}Nd to identify the one-quadrupole-phonon $2_{1,\text{ms}}^+$ state. In total 14 γ-ray transitions were observed, ten of them additionally in coincidence spectra, and assigned to the decay of ten excited states of ^{140}Nd. The identifications of the 2_3^+ state as the main fragment and the 2_4^+ state, at most, as the small fragment of the $2_{1,\text{ms}}^+$ state of ^{140}Nd is based on the determined absolute $M1$ transition strengths,
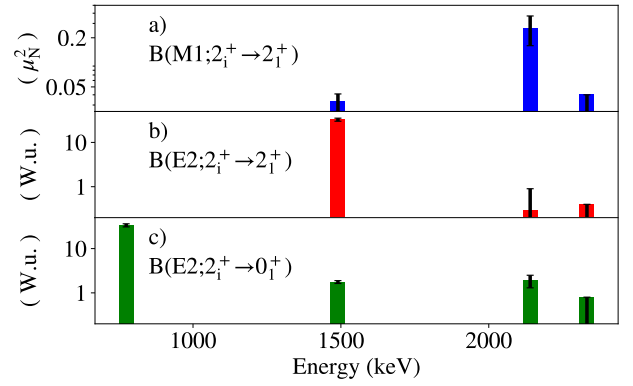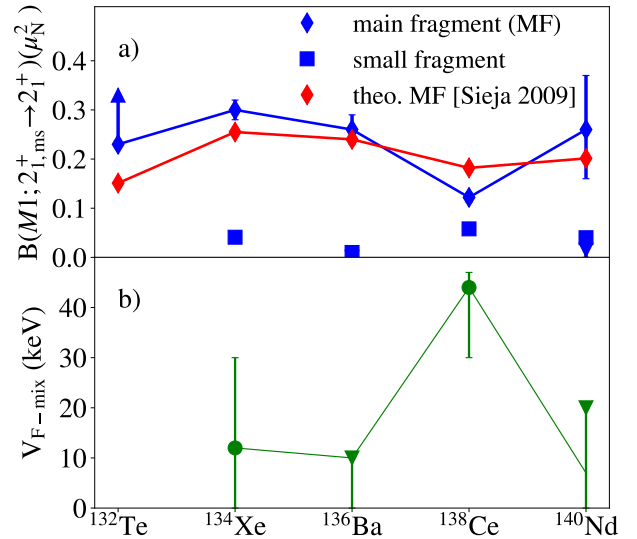
B($M1; 2_3^+ \to 2_1^+$) $= 0.26^{+0.11}_{-0.10}\,\mu_N^2$, B($M1; 2_2^+ \to 2_1^+$) $= 0.033\,(8)\,\mu_N^2$, and B($M1; 2_4^+ \to 2_1^+$) $< 0.04\,\mu_N^2$. The corresponding F-spin mixing matrix element $V_{\text{F}-\text{mix}} < 7^{+13}_{-7}$ keV shows a significant decrease of the F-spin mixing strength from ^{138}Ce to ^{140}Nd. This evolution and the $M1$ strength concentrated to a large extent in the $2_3^+ \to 2_1^+$ transition indicate the restorationn the $valence$-$shell\ stabilization$ after the sub-shell closure at $Z = 58$ for the $N = 80$ isotones at ^{140}Nd ($Z = 60$).

[1] M.G. Mayer, Phys. Rev. **78**, 16 (1950).

[2] R.F. Casten, Phys. Lett. B **152**, 145 (1985).

[3] T. Otsuka, Y. Tsunoda, T. Abe, N. Shimizu, and P. Van Duppen, Phys. Rev. Lett. **123**, 222502 (2019).

[4] A. Bohr and B. Mottelson, *Nuclear Structure* (Benjamin, Reading, MA, 1975), Vol. II.

[5] A. Arima, T. Ohtsuka, F. Iachello, I. Talmi, Phys. Lett. B **66**, 205 (1977).

[6] F. Iachello, Phys. Rev. Lett. **53** 1427 (1984).

[7] D. Bohle, A. Richter, W. Steffen, A.E.L. Dieperink, N. LoIudice, F. Palumbo, O. Scholten, Phys. Lett. B **137** 27 (1984).

[8] N. Pietralla, P. von Brentano, A.F. Lisetskiy, Prog. Part. Nucl. Phys **60** 225-282 (2008).

[9] G. Rainovski, N. Pietralla, T. Ahn, C.J. Lister, R.V.F. Janssens, M.P. Carpenter, S. Zhu and C.J. Barton, Phys. Rev. Lett. **96**, 122501 (2006).

[10] T. Ahn, L. Coquard, N. Pietralla, G. Rainovski, A. Costin, R.V.F. Janssens, C.J. Lister, M.P. Carpenter, S. Zhu, K. Heyde, Phys. Lett. B **679**, 19 (2009).

[11] M. Danchev, G. Rainovski, N. Pietralla, A. Gargano, A. Covello, C. Baktash et al., Phys. Rev. C **84**, 061306(R) (2011).

[12] N. Pietralla, D. Belic, P. von Brentano, C. Fransen, R.-D. Herzberg, U. Kneissl, H. Maser, P. Matschinsky, A. Nord, T. Otsuka, H. H. Pitz, V. Werner, and I. Wiedenhöver, Phys. Rev. C **58**, 796 (1998).

[13] K. Moschner, A. Blazhev, J. Jolie, N. Warr, P. Boutachkov, P. Bednarczyk, et al., Phys. Rev. C **94**, 054323 (2016).

[14] V. Vaquero, A. Jungclaus, P. Doornenbal, K. Wimmer, A.M. Moro, K. Ogata, et al., Phys. Rev. C **99**, 034306 (2019).

[15] M. J. G. Borge and K. Riisager, Eur. Phys. J. A **52**, 334(2016).

[16] Y. Kadi, Y. Blumenfeld, W. Venturini Delsolaro, M.A. Fraser, M. Huyse, A. Papageorgiou Koufidou, J.A. Rodriguez and F. Wenander, J. Phys. G **44**, 084003 (2017).

[17] F. Wenander, J. Instrument. **5**, C10004 (2010).

[18] V.N. Fedosseev, L.-E. Berg, N. Lebas, O.J. Launila, M. Lindroos, R. Losito, B.A. Marsh, F.K. Österdahl, T. Pauchard, G. Tranströmer, J. Vannesjö, Nucl. Instr. and Methods in Phys. Res. B **266**, 4378 - 4382 (2008).

[19] N. Warr, J. Van de Walle, M. Albers, F. Ames, B. Bastin, C. Bauer, et al., Eur. Phys. J. A **49**, 40 (2013).

[20] A.N. Ostrowski, S. Cherubini, T. Davinson, D. Groombridge, A.M. Laird, A. Musumarra, A. Ninane, A. di Pietro, A.C. Shotter, P.J. Woods, Nucl. Instrum. Methods A **480**, 448 (2002).

[21] D. Cline, Ann. Rev. Nucl. Part. Sci. **36**, 683 (1986).

[22] L.P. Gaffney, J. Konki, MiniballCoulexSort, https://doi.org/10.5281/zenodo.1344355 (2019).

[23] T. Czosnyka and C.Y. Whu, Bulletin of the American Physical Society **28**, 745 (1983).

[24] T. Kibédi, T.W. Burrows, M.B. Trzhaskovskaya, P.M. Davidson, C.W. Nestor Jr., Nucl. Instr. and Methods in Phys. Res. Sec. A **589**, 202 (2008).

[25] J. F. Ziegler, M.D. Ziegler and J.P. Biersack, Nucl. Instr. Meth. B, **268**, 1823 (2010).

[26] C. Bauer, G. Rainovski, N. Pietralla, D. Bianco, A. Blazhev, T. Bloch et al., Phys. Rev. C **88**, 021302(R) (2013).

[27] E. Williams, R. J. Casperson, V. Werner, H. Ai, P. Boutachkov, M. Chamberlain, G. Gürdal, A. Heinz, E. A. McCutchan, J. Qian, and R. Winkler, Phys. Rev. C **80**, 054309 (2009).

[28] N. Nica, Nucl. Dat. Sh. **154**, 1-403 (2018).

[29] R.J. Casperson, Dissertation, Yale University (2010).

[30] K.A. Gladnishki, G. Rainovski, P. Petkov, J. Jolie, N. Pietralla, A. Blazhev et al., Phys. Rev. C **82**, 037302 (2010).

[31] G.G. Kennedy, S.C. Gujrathi and S.K. Mark, Z. Phys. A **274**, 233-239 (1975).

[32] D. Bianco, F. Andreozzi, N. LoIudice, A. Porrino and F. Knapp, Phys. Rev. C **85**, 034332 (2012).

[33] K. Sieja, G. Martinez-Pinedo, L. Coquard, N. Pietralla, Phys. Rev. C **80**, 054311 (2009).

[34] N. Lo Iudice, Ch. Stoyanov, D. Tarpanov, Phys. Rev. C **77**, 044310 (2008).